Carbon Capture and Separation from $CO_2/N_2/H_2O$ Gaseous Mixtures in Bilayer Graphtriyne: A Molecular Dynamics Study

Noelia Faginas-Lago[1(✉)], Yusuf Bramastya Apriliyanto[2], and Andrea Lombardi[1]

[1] Dipartimento di Chimica, Biologia e Biotecnologie, Università degli Studi di Perugia, Via Elce di Sotto 8, 06123 Perugia, Italy
noelia.faginaslago@unipg.it
[2] Department of Chemistry, IPB University, Jl Tanjung Kampus IPB Dramaga, 16680 Bogor, Indonesia

Abstract. Molecular dynamics simulations have been performed for CO_2 capture and separation from $CO_2/N_2/H_2O$ gaseous mixtures in bilayer graphtriyne. The gas uptake capacity, permeability as well as selectivity of the layers were simulated based on an improved formulation of force fields tested on accurate *ab initio* calculations on specific systems for mixture separation in post-combustion process. The effect of pressure and temperature on the separation performances of graphtriyne layers was investigated. Compared with the single layer graphtriyne, bilayer graphtriyne can adsorb more molecules with relatively good selectivity, due to the action of the interlayer region as an adsorption site. The interlayer adsorption selectivity of CO_2/N_2 and CO_2/H_2O at a temperature of 333 K and a pressure of 4 atm have been found to be equal to about 20.23 and 1.85, respectively. We also observed that the bilayer graphtriyne membrane has high CO_2 and H_2O permeances compared to N_2, with permeance selectivity ranging from 4.8 to 6.5. Moreover, we found that permeation and adsorption depend on the applied temperature; at high temperatures, permeation and adsorption tend to decrease for all molecules.

Keywords: MD simulations · Graphynes · Carbon capture and separation · Selectivity

1 Introduction

Gas adsorption by porous materials as a phenomenon to ground technologies aimed at reducing greenhouse gas emissions has actively been investigated in the past few years [1–3]. All of these efforts are eventually directed to mitigate possible anthropic contributions to climate change and global warming. Among the greenhouse gases, CO_2 is the most abundant and is regularly released into the atmosphere [4]. Therefore, post-combustion CO_2 capture and separation are important to control the CO_2 emission mainly produced from fossil fuels combustion. Major advantages of porous materials over the traditional aqueous chemical absorbent are in terms of its simplicity, recovery and low implementation costs [5]. Carbon-based materials bearing intrinsic pores

© Springer Nature Switzerland AG 2020
O. Gervasi et al. (Eds.): ICCSA 2020, LNCS 12255, pp. 489–501, 2020.
https://doi.org/10.1007/978-3-030-58820-5_36

currently emerge as potential solid adsorbent candidates for CO_2 capture [6–8]. Unlike other porous materials (e.g. MOFs and polymers), carbon-based materials are hydrophobic, chemically inert and thermally stable. Thanks to their exceptional properties, carbon-based materials are not susceptible to heat and water vapour, which is a characteristic of post-combustion flue gas. Moreover, compared with MOFs and zeolites, carbon-based materials are constructed from lightweight elements linked by strong covalent bonds producing low density and robust structures [9–13]. Therefore, carbon-based materials are economically suitable and viable for post combustion CO_2 capture and separation.

Instead of only capture CO_2 molecules by surface adsorption, two-dimensional carbon-based membranes provide a unique properties harnessed from a combination of surface adsorption and their intrinsic pores acting as molecular sieving to separate CO_2 from other gaseous mixtures [14, 15]. Graphene, a class of carbon-based materials, have been attracting much attention in recent years. It is a single atom thick planar membrane with remarkable properties [16–18]. Surface functionalization by introducing holes or attaching different organic groups is commonly performed in order to modify graphene to meet the requirements for a specific application. For gas adsorption and separation, nano-porous graphene is reported as a promising porous membrane material based on carbon [19, 20]. However, a major drawback of nano-porous graphene is the tendency to form aggregates that limits its gas uptake capacity. Moreover, practically, it is difficult to control the pore size and the homogeneity of their distribution. Analogous with the graphene, γ-graphynes are single atomic layers belonging to the class of carbon allotropes. The carbon atoms in γ-graphynes are arranged as a function of the C-C triple bonds bridging two adjacent hexagons. Possessing similar properties with graphene, γ-graphynes have uniformly distributed and adjustable pores [21–23]. In addition, with lower dispersion forces and therefore a reduced tendency to form aggregates, γ-graphynes are suited for gas capture and separation [24, 25].

Since synthesis and characterization techniques of graphynes are still actively being developed [26–29], computer modelling and simulations play an important role in the material development and evaluation of their performance for gas capture and separation [30, 31]. Recent studies reported that graphtriyne (a form of graphynes, in which each benzene ring is connected to each of six others through a chain composed by three acetylenic bonds), showed a strong physisorption of CO_2 over N_2 and H_2O molecules [32, 33]. It is also reported that the adsorption energy of CO_2 can be enhanced by introducing a new layer of graphtriyne over an existing graphtriyne membrane and so on. The multi-layered graphtriyne systems introduce interlayer spaces that can confine CO_2 molecules trough strong attractive forces. These interlayer spaces can be exploited as new adsorption sites thus the uptake capacity of CO_2 can be increased [34]. In this work, a study of the performance of bilayer graphtriyne membrane for CO_2 capture and separation is evaluated using extended molecular dynamics (MD) simulations. A wide range of relevant conditions in post combustion involving a gaseous mixture of CO_2/N_2/H_2O has been applied in the molecular simulations.

2 Methods

For modelling the intermolecular interactions, the total potential energy of the system is split into electrostatic and non-electrostatic contributions. The total potential energy represents the sum of the intermolecular potential energy between any interacting pair in the system involving CO_2, N_2, H_2O and graphtriyne layers. The electrostatic contribution is calculated using a standard Coulombic summation, by assigning point charges to the interacting molecules. Meanwhile, the non-electrostatic term is expressed using the Improved Lennard-Jones (ILJ) potential [35], as follows:

$$V_{tot}(r) = \sum_{i,j}^{n} \frac{q_i q_j}{r_{ij}} + \sum_{i}^{n} V_{ILJ}(r_i)$$

where

$$V_{ILJ}(r_i) = \varepsilon \left[\frac{m}{n(r) - m} \left(\frac{r_0}{r} \right)^{n(r)} - \frac{n(r)}{n(r) - m} \left(\frac{r_0}{r} \right)^{m} \right]$$

with

$$n(r) = \beta + 4.0 \left(\frac{r}{r_0} \right)^2$$

As can be seen from the above equations, the ILJ potential requires four parameters (r_0, ε, m and β) to be specified. The r_0 and ε are pair specific parameters representing the equilibrium distance and the depth of the potential well, respectively. The m parameter takes the value of 6 for describing interactions between neutral molecules, while the dimensionless β is a parameter that can be adjusted following the hardness of the interaction. The β parameter also corrects the dependence of the interaction on the internuclear distance, improving the potential function at the asymptotic region. The ILJ function so formulated versatile improves the energy profile at equilibrium distance and at short and long range compared to the traditional Lennard-Jones (LJ) function. For a full account of the advantages of the ILJ function see Refs [36–42] and references therein. All of the ILJ parameters used in this report were improved and tested in comparison with high level *ab initio* calculations as reported in the Ref [34]. Figure 1 shows molecular models that represent the gas molecules. These molecular models along with their point charge distributions are adopted from Ref [41–45], where di- and quadrupole moments of the molecules have been considered.

The MD simulations were performed in a simulation box with dimension $72.210 \times 62.523 \times 280.0$ Å^3. The $CO_2/N_2/H_2O$ gaseous mixture with equal fractions of CO_2, N_2 and H_2O molecules was generated randomly distributing the molecules inside the simulation box. A bilayered-graphtriyne membrane with a dimension of 72.210×62.523 Å^2 was placed in the middle of the box (see Fig. 2). The molecular structure of graphtriyne used for the MD simulations is presented in Fig. 3. The graphtriyne structure were optimized by means of periodic density functional theory

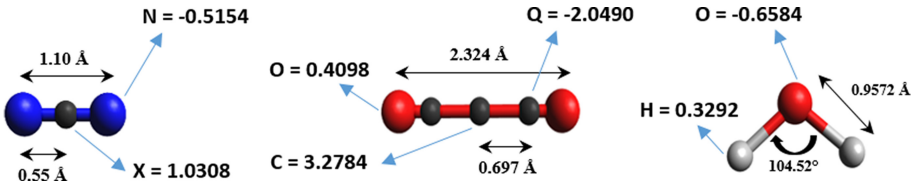


Fig. 1. The models used to represent nitrogen, carbon dioxide and water molecules along with their point charges (e). Q is a point charge representing the C–O bond of CO_2 while X is a point charge representing the N–N bond of N_2.

(DFT) [33]. Seven different amounts of gas molecules have been loaded into the box for the simulations, to investigate the influence of pressure to the gaseous mixtures. The amount of gas molecules inside the box was directly proportional to the initial gas pressure, according to the Peng-Robinson equation of state [46]. In order to mimic post-combustion conditions, four different temperatures (i.e. 333, 353, 373 and 400 K) were considered with initial pressures at relatively low pressure, below 5.5 atm.

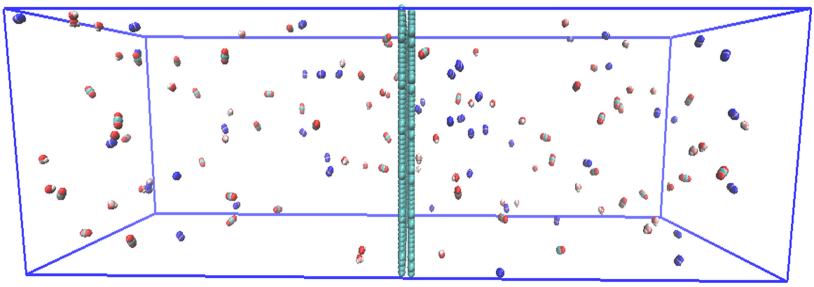


Fig. 2. A snapshot of the simulation box loaded with $CO_2/N_2/H_2O$ mixtures. The graphytriyne is represented by cyan layers located at the centre of simulation box. The cyan and red molecules are CO_2, the blue molecules are N_2, while H_2O is represented by red and white molecules. (Color figure online)

The cut-off distances for the ILJ and electrostatic interactions were set to 15 Å, and the Ewald sum method was applied for the calculation of the electrostatic interactions. The graphtriyne layers were considered as a frozen framework and the gas molecules were treated as rigid bodies. Each simulation was performed for 5.5 ns after a 0.5 ns equilibration period with a fixed time step of 1 fs. The statistical data and trajectory were collected at every 2 ps. The gas molecules could cross the layers multiple times in both directions during the simulation. The number of permeation events was then monitored along calculating the z-density and the radial distribution function profiles. All the MD simulations were performed by using DL_POLY package [47] in the canonical (NVT) ensemble employing the Nose-Hoover algorithm to maintain the applied temperatures. Periodic boundary conditions were implemented in x, y and z directions. The graphical representations and the molecular trajectories were processed by using the VMD program [48].

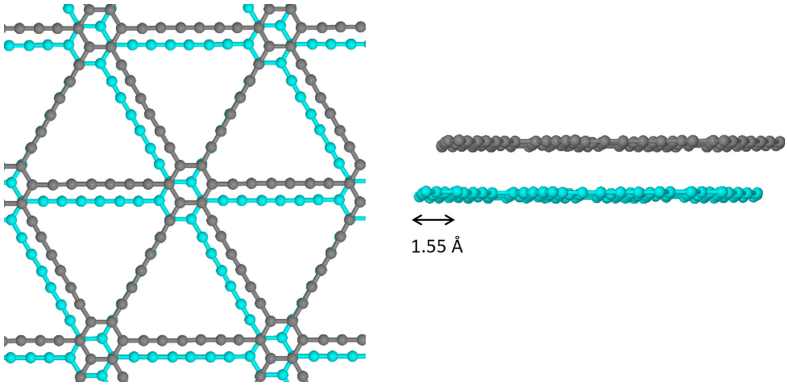


Fig. 3. Top and side views of the bilayer graphtriyne structure. According to the structure predicted by the periodic DFT optimization, one of the carbon sheets is shifted of 1.55 Å with respect to the other sheet [33].

3 Results and Discussions

3.1 Gas Permeability

Production runs of each system were started after 0.5 ns equilibration time. The energy and temperature convergence were checked as an indication of the equilibrated system. The number of permeation events occurred during the production runs was counted and plotted as a function of the simulation time. The slope of this plot is an estimation of the gas permeation rate measured in units of molecules ps^{-1}. Left panel of Fig. 4 shows the permeation events as a function of time for a system simulated at 3.18 atm and 333 K. It can be seen that CO_2 has a higher permeation rate than H_2O and N_2. The high permeation rate of CO_2 can be verified by looking at the radial distribution function profiles that are presented in the right panel of Fig. 4. CO_2 has the largest and highest peaks meaning that CO_2 is more likely to be located near the C atoms of graphtriyne. Consequently, CO_2 molecules have the highest probability to permeate the graphtriyne layers. N_2 has the lowest permeation due to small number of N_2 molecules found near the layers.

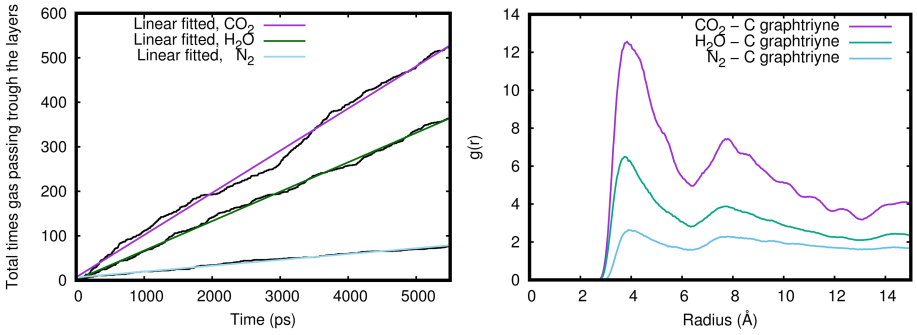


Fig. 4. Permeation events (left) and radial distribution functions (right) at 3.18 atm and 333 K.

Furthermore, knowing the permeation rate, the gas permeance can be calculated by dividing it by the corresponding pressure and area of the graphtriyne layers. The gas permeances were reported in gas permeance unit (GPU) (1 GPU = 3.35×10^{-10} mol m^{-2} s^{-1} Pa^{-1}). In order to widen the applied conditions, we also performed MD simulations at seven different pressures and four different temperatures. The results are reported in Fig. 5. Figure 5, left panel, shows that N_2 permeances are slightly affected by the pressures. On the other hand, CO_2 and H_2O permeances tend to decrease as the pressure increases. From these data, the average of gas permeances were calculated and then plotted as a function of temperature (Fig. 5, right panel). It was observed that the average of gas permeance for all gas decreases with the increasing of temperature. This phenomenon is indeed related to their kinetic energy as the temperature varies. The higher is the kinetic energy, the higher is the velocity of molecules to compete with attraction forces of the layers. A high temperature decreases gas permeance by minimizing attraction effects to steer gas molecules toward the graphtriyne layers. The gas permeation reported in Fig. 5 is in a good agreement with the potential energy curves reported by Bartolomei and co-workers [33], where well depths increase according to the sequence N_2, H_2O, CO_2 (highest value). Although CO_2 has a deeper potential well than H_2O, the average gas permeances for CO_2 and H_2O are comparable. This fact is closely related with the stereoselective requirement for CO_2 to pass through the layers as already discussed in Ref [34]. Nevertheless, by including also the deviation into our consideration (Fig. 5), we can say that CO_2 still has the highest gas permeance. For the case of N_2, low N_2 permeance at all temperatures indicates that attraction force of the graphtriyne layers to N_2 is too weak compared to that of CO_2 and H_2O.

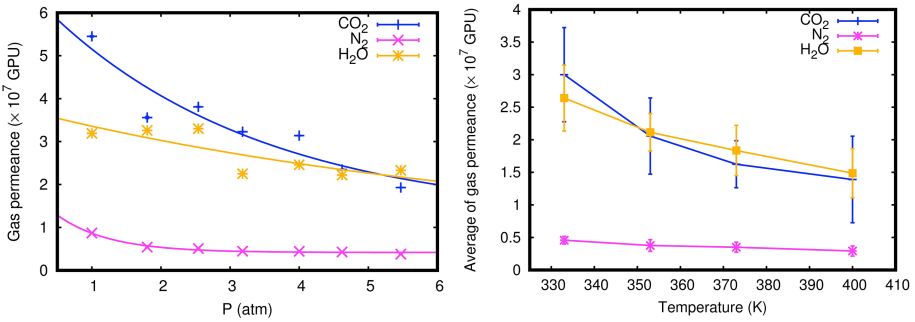


Fig. 5. Gas permeance at 333 K (left panel) and average of gas permeance as a function of temperature (right panel).

Although the data presented in Fig. 5 follow a similar trend as reported in the Ref [34], the gas permeances in this report are relatively lower (ranging from 0.6 to 3.0 $\times$ 10^7 GPU and 0.3 to 0.6 $\times$ 10^7 GPU for CO_2 and N_2 respectively). Low values of gas permeances are caused by more competitions existing between the $CO_2/N_2/H_2O$ gaseous mixtures when interacting with graphtriyne. Moreover, the temperatures applied in this report are also higher. Furthermore, by comparing the average of gas permeances

obtained for all type of systems, we calculated permeance selectivities and plotted the values as function of temperature (Fig. 6). In general, temperature slightly affects the permeance selectivity of all pairs. Permeance selectivity values of H_2O/N_2 overlap with those of CO_2/N_2 by having similar values ranging from 4.8 to 6.5. On the other hand, H_2O/CO_2 selectivity is around 1 which implies that the bilayer graphtriyne membrane is not selective for CO_2–H_2O separation. Although the permeance selectivities are lower than CO_2/N_2 selectivity reported by Liu *et al.* [15] (about 100, with CO_2 permeance = 2.8×10^5 GPU) for nanoporous graphene at 300 K and by Schrier [12] (about 60, with CO_2 permeance = 3×10^5 GPU) for Porous Graphene-E-Stilbene-1 (PG-ES1) at 325 K, the CO_2 permeances for bilayer graphtriyne (ranging from 0.6 to 3.0×10^7 GPU) are two order of magnitudes higher. Nevertheless, the CO_2/N_2 permeance selectivities are comparable to those reported by Wu and co-workers [17] for fluorine modified nano-porous graphene at 300 K (ranging from 4 to 11). It is already known that trade-off issue between selectivity and permeability is a drawback of membrane based-materials. However, its simplicity and efficiency make membrane-based technology still widely used for gas separation [18].

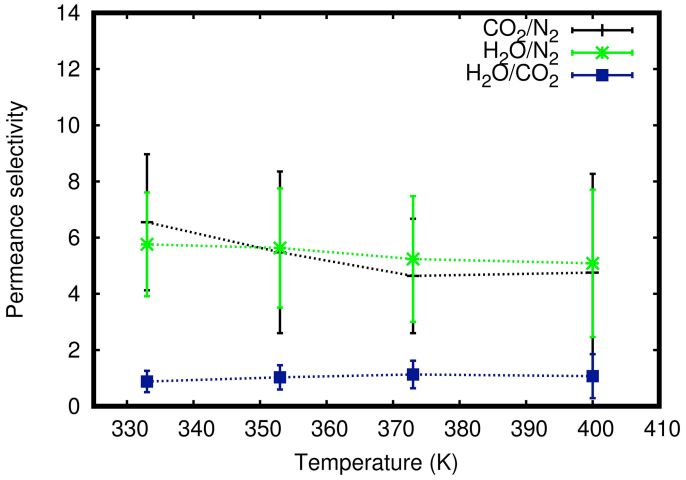


Fig. 6. Permeance selectivity as a function of temperature.

3.2 Gas Adsorption

In addition to the radial distribution functions reported in Fig. 4, the stronger attraction for CO_2 than H_2O and N_2 is also reflected in the z-density profiles presented in Fig. 7. The z-density is a plot of the mean number density of gas along the z-axis, where the z-axis is perpendicular with the graphtriyne layers. The highest peaks of CO_2 indicate that graphtriyne layers exhibit strong adsorption of CO_2, especially inside the interlayer region. The z-density profiles also present sharp peaks outside the layers at a distance of around 3.4 Å from the surface for all gas molecules. Figure 7 also shows that the interlayer region is selective for CO_2 uptake and separation from the $CO_2/H_2O/N_2$

gaseous mixture. For instance, at 333 K and 4 atm, we obtained interlayer adsorption selectivity of CO_2/N_2 and CO_2/H_2O about 20.23 and 1.85 respectively. High and broad peaks of CO_2 presented in Fig. 7 correspond to the deep and wide of CO_2 potential well, meaning a strong long ranged attractions. Therefore, compared with the single layer, the bilayer graphriyne membrane adsorbs more molecules facilitated by their interlayer pores [32]. As already discussed before, the permeation events are closely related to the adsorption of gas over the surfaces of membrane. The more gas is adsorbed over the surfaces, the more probable is the gas to cross the layers. However, the amount of adsorbed molecules in the interlayer region also can diminish the gas permeance by saturating the pores and blocking other molecules to cross the membrane. This phenomenon happens for the case of CO_2, where the attraction forces are very strong in the interlayer region. Beside the stereodynamic requirement of CO_2 to cross the layers, permeation events of CO_2 were also inhibited by other CO_2 molecules that occupied the intermolecular pores. Consequently, the average of CO_2 permeances are relatively low and comparable with those of H_2O (Fig. 5, right panel) even though a lot of CO_2 molecules were adsorbed at the surfaces of graphtriyne.

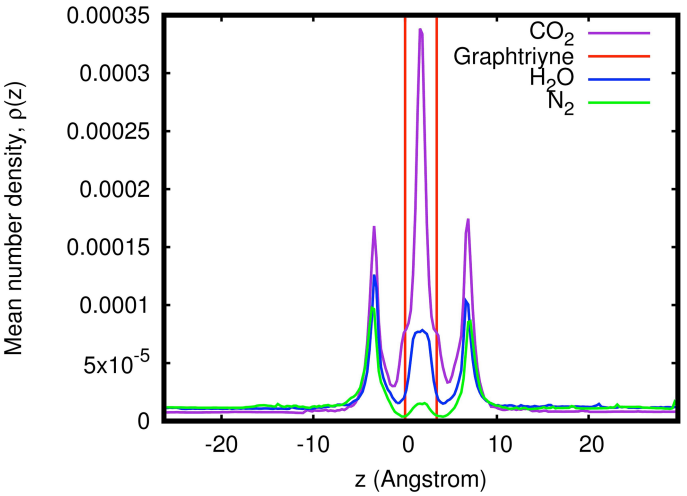


Fig. 7. Z-density profiles simulated at 1.8 atm and 353 K.

We also calculated the total gas uptakes by integrating the z-density profiles at the adsorption region. The adsorption region is the area under the z-density peaks, in which located in the range of 6.9 Å from the surface of graphtriyne including the area between the layers presented in the z-density profiles. The gas uptakes at 333 K for all applied pressures were presented in the left panel of Fig. 8 as adsorption isotherms. It can be seen that the gas uptake is linearly proportional to the initial pressure; the higher is the initial pressure, the higher is the gas uptake value. The linear trend has been expected since the MD simulations are conducted at low pressures regimes, where the gas molecules have not saturate the adsorption sites. Furthermore, by calculating the slope

of adsorption isotherms, we estimated the adsorption coefficient of each systems. The adsorption coefficients for all molecules are reported in the right panel of Fig. 8 as a function of temperature. Figure 8 shows that CO_2 has the highest gas uptakes and adsorption coefficients among gas molecules. The adsorption coefficients decrease as the increasing of temperature for all gas molecules. It can be expected that gas physisorption is relatively ineffective at high temperatures. Weak attraction of N_2 is manifested by the fact that N_2 has the lowest adsorption coefficients (about 0.02 to 0.04 mmol g^{-1} atm^{-1}). Low uptake of N_2 caused low permeance values of N_2 as presented in Fig. 5.

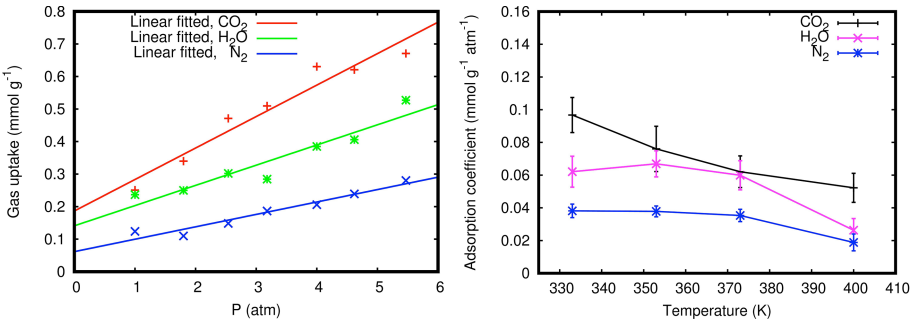


Fig. 8. Adsorption isotherm profiles at 333 K (left panel) and adsorption coefficient as a function of temperature (right panel).

Adsorption selectivity of graphtriyne layers were reported in term of total adsorption selectivity. The total adsorption refers to the sum of the interlayer adsorption and the surface adsorption. The total adsorption selectivity $S_{ads}^{A/B}$ were calculated as the following,

$$S_{ads}^{A/B} = \frac{n_{A(ads)}}{n_{A(free)}} \times \frac{n_{B(free)}}{n_{B(ads)}}$$

$n_{A(ads)}$ and $n_{B(ads)}$ are the numbers of adsorbed molecules A and B, while $n_{A(free)}$ and $n_{B(free)}$ are the numbers of free molecules A and B, respectively. The total adsorption selectivity for all systems are provided in Table 1. In general, total adsorption selectivity of all gas pairs decreases as the increasing of pressure and temperature. Table 1 shows that bilayer graphtriyne exhibits relatively high CO_2/N_2 total adsorption selectivity especially at low pressure and temperature. The CO_2/N_2 selectivities reported in Table 1 are higher than those reported in our previous report for the single layer system [32]. We obtained CO_2/N_2 total adsorption selectivities at 373 K for bilayer system ranging from 2.3 to 5.2, while in the previous work for single layer system are in the range of 1.3 to 2.4 at the same temperature. However, the bilayer graphtriyne is not selective enough for CO_2/H_2O adsorption with total selectivity values ranging from 1 to 2 for all applied temperatures. It has been reported that competitive adsorption between water vapour and CO_2 on the same adsorption sites of various materials is

observed in post-combustion CO_2 capture and separation [5, 30]. In most cases, H_2O interferences are minimized by condensing the water molecules or by modifying the adsorbent materials to have more hydrophobic surfaces. Nevertheless, doubling the graphtriyne layer can enhance the amount of adsorbed molecules and the selectivity by providing new adsorption sites in the interlayer pores.

Table 1. Total adsorption selectivity of $CO_2/N_2/H_2O$ gaseous mixture

Temperature (K)	Gas	Total adsorption selectivity						
		1.00 atm	1.80 atm	2.54 atm	3.18 atm	4.00 atm	4.62 atm	5.47 atm
333	CO_2/N_2	3.43	4.58	4.67	3.67	4.14	3.26	2.90
	H_2O/N_2	3.00	2.84	2.40	1.65	2.10	1.86	2.12
	CO_2/H_2O	1.14	1.62	1.95	2.22	1.97	1.75	1.37
353	CO_2/N_2	3.19	4.24	3.64	4.19	2.79	2.78	2.60
	H_2O/N_2	2.45	1.69	2.08	2.06	1.88	1.93	1.99
	CO_2/H_2O	1.30	2.51	1.75	2.03	1.48	1.44	1.31
373	CO_2/N_2	5.16	3.04	3.40	2.67	2.62	2.62	2.33
	H_2O/N_2	0.81	3.12	2.05	1.42	2.04	1.59	1.84
	CO_2/H_2O	6.35	0.97	1.65	1.88	1.28	1.65	1.26
400	CO_2/N_2	1.08	3.96	3.12	2.26	2.68	2.54	2.36
	H_2O/N_2	1.87	2.00	1.65	1.57	1.75	1.54	1.57
	CO_2/H_2O	0.58	1.98	1.89	1.44	1.53	1.66	1.50

4 Conclusions

Bilayer graphtriyne has been investigated for the purpose of CO_2 capture and separation materials. The gas uptake capacity and permeability of the layers were simulated computationally employing $CO_2/H_2O/N_2$ gaseous mixture systems in wide range of conditions. Extensive MD simulations were performed based on an improved formulation of force fields. Compared to generic force fields, our formulation was tested on accurate *ab initio* calculations on specific systems for mixture separation and gas capture in post-combustion process. Therefore, a quantitative description of the interactions and realistic results were obtained for the dynamics under considered systems. We observed that the bilayer graphtriyne membrane has high CO_2 and H_2O permeances compared to N_2 with relatively good selectivity (from 4.8 to 6.5). Adsorbed CO_2 molecules lower the CO_2 permeance by occupying the interlayer pores and preventing permeation events. As a result, CO_2 has permeance values similar to H_2O, despite the CO_2 adsorption is more favourable than that of other molecules. High CO_2 uptake capacity and selectivity were founded in the interlayer region. The interlayer adsorption selectivity of CO_2/N_2 and CO_2/H_2O are about 20.23 and 1.85, respectively at 333 K and 4 atm. The layers are not selective enough for CO_2/H_2O capture and separation as also reported for other materials. Nevertheless, in post-combustion application, competitive CO_2/H_2O adsorption can be reduced by condensing H_2O prior interacting the flue gas with the graphtriyne layers. In addition, we also investigated the effect of temperature to the gas uptake capacity, permeability and selectivity. As the temperature

increases; the gas uptake, adsorption coefficient and gas permeance decrease for all gas molecules. Among carbon-based materials, bilayer graphtriyne can be considered as an alternative membrane with its potential properties for mixture separation that offers fast and efficient separation of different molecular species.

Acknowledgements. YBA thanks to the LCPQ - Université de Toulouse III for allocated computing time. NF-L, AL thank MIUR and the University of Perugia for the financial support of the AMIS project through the "Dipartimenti di Eccellenza" programme. N. F.-L. also acknowledges the Fondo Ricerca di Base 2017 (RICBASE2017BALUCANI) del Dipartimento di Chimica, Biologia e Biotecnologie della Università di Perugia for financial support. A. L. acknowledges financial support from MIUR PRIN 2015 (contract 2015F59J3R 002) and the OU Super-computing Center for Education & Research (OSCER) at the University of Oklahoma, for allocated computing time.

References

1. Bui, M., et al.: Carbon capture and storage (CCS): the way forward. Energy Environ. Sci. **11**, 1062–1176 (2018)
2. Huck, J.M., et al.: Evaluating different classes of porous materials for carbon capture. Energy Environ. Sci. **7**, 4132–4146 (2014)
3. Li, J.R., et al.: Porous materials with pre-designed single-molecule traps for CO_2 selective adsorption. Nat. Commun. **4**, 1538 (2013)
4. World Resources Institute (WRI): Climate Analysis Indicators Tool (CAIT): WRI's climate data explorer (2020). http://cait.wri.org. Accessed February 2020
5. Smit, B.: Carbon capture and storage: introductory lecture. Faraday Discuss. **192**, 9–25 (2016)
6. Srinivas, G., Krungleviciute, V., Guo, Z.X., Yildrim, T.: Exceptional CO_2 capture in a hiearchically porous carbon with simultaneous high surface area and pore volume. Energy Environ. Sci. **7**, 335–342 (2014)
7. Ganesan, A., Shaijumon, M.M.: Activated graphene-derived porous carbon with exceptional gas adsorption properties. Microporous Mesoporous Mater. **220**, 21–27 (2016)
8. Ghosh, S., Sevilla, M., Fuertes, A.B., Andreoli, E., Ho, J., Barron, A.R.: Defining a performance map of porous carbon sorbents for high-pressure carbon dioxide uptake and carbon dioxide-methane selectivity. J. Mater. Chem. A **4**, 14739–14751 (2016)
9. Kim, J., Lin, L.C., Swisher, J.A., Haranczyk, M., Smit, B.: Predicting large CO_2 adsorption in aluminosilicate zeolites for postcombustion carbon dioxide capture. J. Am. Chem. Soc. **134**, 18940–18943 (2012)
10. Lin, L.C., et al.: Understanding CO2 dynamics in metal-organic frameworks with open metal sites. Angew. Chem. **125**, 4506–4509 (2013)
11. Queen, W.L., et al.: Comprehensive study of carbon dioxide adsorption in the metal-organic frameworks M2 (dobdc) (M = Mg, Mn, Fe Co, Ni, Cu, Zn). Chem. Sci. **5**, 4569–4581 (2014)
12. Schrier, J.: Carbon dioxide separation with a two-dimensional polymer membrane. ACS Appl. Mater. Interfaces **4**, 3745–3752 (2012)

13. Xiang, Z., et al.: Systematic tuning and multifunctionalization of covalent organic polymers for enhanced carbon capture. J. Am. Chem. Soc. **137**, 13301–13307 (2015)
14. Koenig, S.P., Wang, L., Pellegrino, J., Bunch, S.: Selective molecular sieving trough porous graphene. Nat. Nanotechnol. **7**, 728–732 (2012)
15. Liu, H., Dai, S., Jiang, D.: Insights into CO_2/N_2 separation trough nanoporous graphene from molecular dynamics. Nanoscale **5**, 9984–9987 (2013)
16. Vekeman, J., Cuesta, I.G., Faginas-Lago, N., Wilson, J., Sánchez-Marín, J., de Merás, A.S.: Potential models for the simulation of methane adsorption on graphene: development and CCSD (T) benchmarks. Phys. Chem. Chem. Phys. **20**, 25518–25530 (2018)
17. Wu, T., et al.: Fluorine-modified porous graphene as membrane for CO_2/N_2 separation: molecular dynamic and first-principles simulations. J. Phys. Chem. C **118**, 7369–7376 (2014)
18. Du, H., Li, J., Zhang, J., Su, G., Li, X., Zhao, Y.: Separation of hydrogen and nitrogen gases with porous graphene membrane. J. Phys. Chem. C **115**, 23261–23266 (2011)
19. Tao, Y., et al.: Tunable hydrogen separation in porous graphene membrane: first-principle and molecular dynamic simulation. ACS Appl. Mater. Interfaces **6**, 8048–8058 (2014)
20. Ambrosetti, A., Silvestrelli, P.L.: Gas separation in nanoporous graphene from first principle calculations. J. Phys. Chem. C **118**, 19172–19179 (2014)
21. James, A., et al.: Graphynes: indispensable nanoporous architectures in carbon flatland. RSC Adv. **8**, 22998–23018 (2018)
22. Bartolomei, M., et al.: Penetration barrier of water through graphynes' pores: first-principles predictions and force field optimization. J. Phys. Chem. Lett. **5**, 751–755 (2014)
23. Lin, S., Buehler, M.J.: Mechanics and molecular filtration performance of graphyne nanoweb membranes for selective water purification. Nanoscale **5**, 11801–11807 (2013)
24. Meng, Z., et al.: Graphdiyne as a high-efficiency membrane for separating oxygen from harmful gases: a first-principles study. ACS Appl. Mater. Interfaces **8**, 28166–28170 (2016)
25. Bartolomei, M., Carmona-Novillo, E., Giorgi, G.: First principles investigation of hydrogen physical adsorption on graphynes' layers. Carbon **95**, 1076–1081 (2015)
26. Zhou, J., et al.: Synthesis of graphdiyne nanowalls using acetylenic coupling reaction. J. Am. Chem. Soc. **137**, 7596–7599 (2015)
27. Gao, X., et al.: Ultrathin graphdiyne film on graphene through solution-phase Van Der Waals epitaxy. Sci. Adv. **4**, eaat6378 (2018)
28. Sakamoto, R., et al.: A pyrazine-incorporated graphdiyne nanofilm as a metal-free electrocatalyst for the hydrogen evolution reaction. J. Mater. Chem. A **6**, 22189–22194 (2018)
29. Bao, H., Wang, L., Li, C., Luo, J.: Structural characterization and identification of graphdiyne and graphdiyne-based materials. ACS Appl. Mater. Interfaces. **11**, 2717–2729 (2018)
30. Joos, L., Huck, J.M., Speybroeck, V.V., Smit, B.: Cutting the cost of carbon capture: a case for carbon capture and utilization. Faraday Discuss. **192**, 391–414 (2016)
31. Braun, E., et al.: High-throughput computational screening of nanoporous adsorbents for CO_2 capture from natural gas. Mol. Syst. Des. Eng. **1**, 175–188 (2016)
32. Faginas-Lago, N., Apriliyanto, Y.B., Lombardi, A.: Molecular simulations of $CO_2/N_2/H_2O$ gaseous mixture separation in graphtriyne membrane. In: Misra, S., et al. (eds.) ICCSA 2019. LNCS, vol. 11624, pp. 374–387. Springer, Cham (2019). https://doi.org/10.1007/978-3-030-24311-1_27
33. Bartolomei, M., Giorgi, G.: A novel nanoporous graphite based on graphynes: first-principles structure and carbon dioxide preferential physisorption. ACS Appl. Mater. Interfaces. **8**, 27996–28003 (2016)

34. Apriliyanto, Y.B., et al.: Nanostructure selectivity for molecular adsorption and separation: the case of graphyne layers. J. Phys. Chem. C **122**, 16195–16208 (2018)
35. Pirani, F., Brizi, S., Roncaratti, L.F., Casavecchia, P., Cappelletti, D., Vecchiocattivi, F.: Beyond the Lennard-Jones model: a simple and accurate potential function probed by high resolution scattering data useful for molecular dynamics simulations. Phys. Chem. Chem. Phys. **10**, 5489–5503 (2008)
36. Lago, N.F., Larrañaga, F.H., Albertí, M.: On the suitability of the ILJ function to match different formulations of the electrostatic potential for water-water interactions. Eur. Phys. J. D **55**, 75–85 (2009). https://doi.org/10.1140/epjd/e2009-00215-5
37. Faginas-Lago, N., Yeni, D., Huarte, F., Wang, Y., Alcamí, M., Martin, F.: Adsorption of hydrogen molecules on carbon nanotubes using quantum chemistry and molecular dynamics. J. Phys. Chem. A **120**, 6451–6458 (2016)
38. Faginas-Lago, N., Lombardi, A., Albertí, M., Grossi, G.: Accurate analytic intermolecular potential for the simulation of Na^+ and K^+ ion hydration in liquid water. J. Mol. Liq. **204**, 192–197 (2015)
39. Albertí, M., Lago, N.: Competitive solvation of K^+ by C_6H_6 and H_2O in the K^+-$(C_6H_6)_n$-$(H_2O)_m$ (n = 1–4; m = 1–6) aggregates. Eur. Phys. J. D **67**, 73 (2013). https://doi.org/10.1140/epjd/e2013-30753-x
40. Albertí, M., Faginas Lago, N., Pirani, F.: Ar solvation shells in K^+–HFBz: from cluster rearrangement to solvation dynamics. J. Phys. Chem. A **115**(40), 10871–10879 (2011)
41. Albertí, M., Aguilar, A., Cappelletti, D., Laganà, A., Pirani, F.: On the development of an effective model potential to describe water interaction in neutral and ionic clusters. Int. J. Mass Spectrom. **280**, 50–56 (2009)
42. Lombardi, A., Palazzetti, F.: A comparison of interatomic potentials for rare gas nanoaggregates. J. Mol. Struct. THEOCHEM **852**, 22–29 (2008)
43. Albertí, M., Pirani, F., Lagana, A.: Carbon dioxide clathrate hydrates: selective role of intermolecular interactions and action of the SDS catalyst. J. Phys. Chem. A **117**, 6991–7000 (2013)
44. Lombardi, A., Pirani, F., Laganà, A., Bartolomei, M.: Energy transfer dynamics and kinetics of elementary processes (promoted) by gas-phase CO_2-N_2 collisions: selectivity control by the anisotropy of the interaction. J. Comput. Chem. **37**, 1463–1475 (2016)
45. Bartolomei, M., Pirani, F., Laganà, A., Lombardi, A.: A full dimensional grid empowered simulation of the CO_2 + CO_2 processes. J. Comput. Chem. **33**, 1806–1819 (2012)
46. Elliott, J.R., Lira, C.T.: Introductory Chemical Engineering Thermodynamics, 2nd edn. Prentice Hall, New Jersey (2012)
47. Smith, W., Yong, C., Rodger, P.: DL_POLY: application to molecular simulation. Mol. Simul. **28**, 385–471 (2002)
48. Humphrey, W., Dalke, A., Schulten, K.V.M.D.: Visual molecular dynamics. J. Mol. Graph. **14**, 33–38 (1996)